Advances in the Ignitor Program

B. Coppi 1), A. Airoldi 2), F. Alladio 3), A. Bianchi 4), F. Bombarda 3), A. Capriccioli 3), G. Cenacchi 3), A. Coletti 3), R. Coletti 3), A. Cucchiaro 3), P. Detragiache 3), A. Frattolillo 3), P. Frosi 3), L. Galbiati, F. Lucchini 3), G. Maddaluno 3), R. Maggiora 5), S. Migliori 3), B. Parodi 4), S. Pierattini 3), A. Pizzuto 3), G. Ramogida 3), M. Roccella 3), M. Romanelli 3), M. Santinelli 3), M. Sassi 3), A. Sestero, F. Subba 5), R. Zanino 5)

1) ENEA, Italy;
2) CNR – Istituto Fisica del Plasma, Milan, Italy;
3) Associazione Euratom-ENEA sulla Fusione, Frascati, Italy;
4) Ansaldo Ricerche, Genoa, Italy
5) Politecnico di Torino, Turin, Italy.

e-mail of main author: coppi@mit.edu

Advances in the Ignitor Program*

B. Coppi 1), A. Airoldi 2), F. Alladio 3), A. Bianchi 4), F. Bombarda 3), A. Capriccioli 3), G. Cenacchi 3), A. Coletti 3), R. Coletti 3), A. Cucchiaro 3), P. Detragiache 3), A. Frattolillo 3), P. Frosi 3), L. Galbiati, F. Lucchini 3), G. Maddaluno 3), R. Maggiora 5), S. Migliori 3), B. Parodi 4), S. Pierattini 3), A. Pizzuto 3), G. Ramogida 3), M. Roccella 3), M. Romanelli 3), M. Santinelli 3), M. Sassi 3), A. Sestero, F. Subba 5), R. Zanino 5)

1) ENEA, Italy;
2) CNR – Istituto Fisica del Plasma, Milan, Italy;
3) Associazione Euratom-ENEA sulla Fusione, Frascati, Italy;
4) Ansaldo Ricerche, Genoa, Italy
5) Politecnico di Torino, Turin, Italy.
e-mail of main author: coppi@mit.edu

Abstract

The most significant recent advances that have been made within the Ignitor program are described. For physics, these involve the analysis of the confinement properties of plasmas produced in recent experiments with peaked density profiles relevant to Ignitor, the characterization of the regimes with double X-point configurations that Ignitor can generate, and the study of oscillatory states for the plasma pressure near ignition that can be obtained by both external and internal forms of control. On the engineering side, the second generation prototypes of the toroidal magnet plates that have been constructed are described. The completion of the design of the plasma chamber that withstands the estimated disruption forces, of the first wall system, including Mo tiles and associated supporting plates, and of the remote handling system is reported. Other relevant R&D activities (i.e. construction of a fast pellet injector) are being carried out. The design of all elements of the poloidal field system has been re-optimized. The analysis of the connection of Ignitor to a node of the European grid has been completed with positive results and official authorization. The set of currents in the machine coils, for a plasma current pulse of 11 MA, that minimizes the requirements of the machine electrical power supply system has been identified.

1. Ignition and Relevant Experimental Observations

Ignition, the condition where the nuclear plasma heating equals the rate of plasma energy loss, can be attained at relatively low peak temperatures in a high magnetic field experiment, such as Ignitor [1] (R_0=1.32 m, $a{\times}b \simeq 0.47{\times}0.86$ m^2, $B_T \lesssim 13$ T, $I_p \lesssim 11$ MA), designed to explore the physics of burning plasmas. In the reference operation scenario the plasma current reaches its maximum value in 4 s and the subsequent flattop lasts 4 s. A number of simulations carried out by the JETTO transport code [2,3] to study the attainment of ignition have pointed out that Ignitor can reach its goals by operating in regimes where no pressure pedestal is formed at the edge of the plasma column.

The most accessible conditions to reach ignition involve relatively peaked density profiles (e.g., $n_0/\langle n \rangle \cong 2$) as they are beneficial for fusion burning plasmas from several perspectives, and in particular can provide a stability edge against the so-called η_i modes that enhance the ion thermal transport. In fact, the injection of pellets to prevent the confinement saturation was suggested originally for the Alcator C experiments to stabilize the Ion Temperature Gradient (ITG) driven modes by means of an adequate density gradient. Density profile peaking produced by multiple pellet injection have sustained enhanced confinement regimes in experiments carried out on the FTU machine [4]. As already observed in earlier experiments, the confinement time τ_E increases with density up to a saturation value, corresponding to the so-called L-mode regime,

when the density profiles are relatively flat [5]. This saturation occurs at about half the value of the "density limit". Following the injection of pellets, the positive trend of the neo-Alcator scaling with density is extended; τ_E reaches values in excess of 100 ms [6] at $I_p \cong 0.8$ MA and $B_T \cong 7.2$ T, with a significant overall improvement above the saturation level, for n_{e0} as high as 8×10^{20} m^{-3}, close to the Ignitor reference central density, with a density peaking factor above 3. The product $n_0 \tau_E$ reaches about 10^{20} sec/m^3 and the corresponding effective thermal diffusivity $\chi^E \cong a^2/4\tau_E \cong 0.2$ m^2/s is within the range of the values estimated for Ignitor in order to reach ignition. The suppression of sawtooth activity brings to impurity occumulation, and the plasma returns to a lower confinement level within 50 ms. On the other hand, at higher current (1.1 MA), impurity accumulation is avoided thanks to the persistence of a slower (relative to the pre-pellet phase) sawtooth activity [4]; the increase of both confinement time and density peaking in this case is modest, but considerably more stable.

Extrapolations of the FTU ohmic regimes to the case of Ignitor is not straightforward, since the plasma current is higher by more than a factor of 10 (the average poloidal magnetic pressure in Ignitor is about 25 times the FTU value at 1 MA) but the plasma temperature is also ten times higher, bringing ν^* to a lower value than in FTU. The line average density at ignition is less than half the density limit, and therefore the confinement time can be expected to be as high as it can be before reaching saturation. The density peaking, on the other hand, is similar to that observed on FTU at the lowest densities and currents.

In order to control density peaking, a high speed, multiple pellet injector [7] is planned as an integral part of the Ignitor facility. The ENEA Laboratory at Frascati and the Fusion Technology Group of Oak Ridge are jointly developing a multiple injector capable of shooting pellets of variable sizes for Ignitor. The initial activities are devoted to the construction of a 4 barrel, double stage gun able to reach speeds up to 4 km/s. Previous simulations indicate that speeds of 3-4 km/s would allow a sufficient particle penetration within the plasma column, particularly during the initial current rise, when the plasma temperature is lower but density profile control is more desirable. The compact size of the Ignitor machine favors the injection from the low field side, for which very positive results have been obtained on the FTU machine, in terms of density profile peaking and good energy confinement. The ongoing activities include the procurement of all the hardware for the cryocooler, diagnostics and control electronics, from the ORNL side, and the design and construction of the gun by ENEA. A new fast valve has been developed that considerably reduces the requirements on the expansion volumes necessary to prevent the propulsion gas to reach the plasma chamber.

2. H-mode

The possibility of exploiting the characteristics of the H-mode regime in Ignitor to reach conditions close to ignition has been confirmed for a double null configuration with the X-points laying on the first wall and with $I_p \cong 9$ MA, and $a \cong 0.44$ m. A 0-D analysis of the operating space with H-mode confinement has been performed, solving the global power balance equation for a given value of the gain parameter $Q = P_{fus}/(P_{OH} + P_{aux})$. Confinement is assumed to scale as ITER98(y,2) when the heating power P_{heat} exceeds the threshold value P_{thr} given in Ref. [8] by a factor 1.3. An impurity concentration of 1.2% for B and 10^{-5} for Mo was chosen, so that $Z_{eff} = 1.3$ in the presence of alpha particle ashes with a concentration of 2.0%. With a modest profile peaking for density ($n_0/\langle n \rangle = 1.25$) and a midrange one for temperature ($T_0/\langle T \rangle = 2.5$), operation at high-$Q$ appears possible. The operating space (defined by the condition $1.3 \times P_{thr} < P_{heat} < 30$ MW) is shown in Fig. 1 for $Q = 30$. An interesting operating point is the one with $n_{e0} = 6.3 \times 10^{20}$ m^{-3} and $T_{e0} = 16.4$ keV, corresponding to $P_\alpha = 25$ MW and values of normalized density $\bar{n}/n_G = 0.37$ and normalized beta ($\beta_N = 1.1$)

well below those corresponding to tokamak operating limits. Assuming flatter pressure profiles $(n_0/\langle n\rangle = 1.1$ and $T_0/\langle T\rangle = 2.0)$, operation becomes limited to values of Q up to 10.

The electromagnetic, thermal and structural analysis for these configurations has been carried out using FEM models (2D for electromagnetic and 3D for thermal and structural calculations), which includes an accurate description of the geometry and the materials of each component of the machine core. The resulting in-plane stresses are comparable to those of the reference limiter configuration.
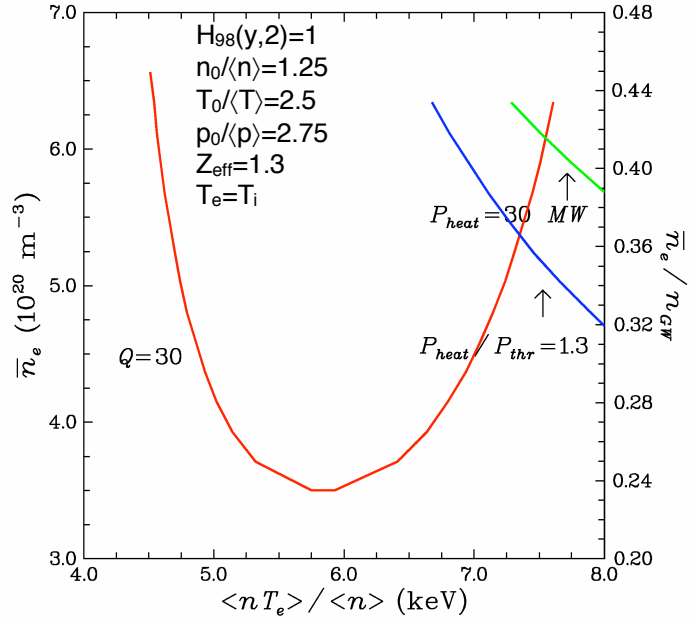

Fig. 1- Operating space for H-mode regimes in Ignitor

3. Quasi-Steady State Conditions

We have studied representative discharges where oscillatory states are maintained near ignition with the JETTO code. The relevant MHD equilibria are evaluated and coupled to the transport equations for the toroidal current density, the electron and ion thermal energies, the plasma fuel densities and two impurity ion densities. One of the adopted electron thermal transport models is based on a semiempirical Bohm-gyroBohm expression [9] for the electron thermal conductivity that has been used previously to reproduce a range of relevant experimental observations, and specifically those obtained by the FTU machine in the presence of electron cyclotron heating at high density [10]. The ion diffusivity is taken as $\chi_i=\chi_{NC}+0.05\chi_e$ and the particle diffusion is represented by $D_p = 0.23\chi_e$. Sawtooth oscillations are treated by a complete reconnection model (that is pessimistic according to theory as well as experimental indications), triggered by an assigned value of the pressure peaking factor. The ICRH power injection process is represented including the width of the deposition region, the application time and the total absorbed power [11].

In the fusion burning regimes presented here, the fusion gain is toned down by combining the RF pulse and the tritium inflow, but ignition is not the goal of these simulations, given that this has been proven in previous analyses [1]. In the first case (Pulse #040714a), tritium is fed 2 s after the discharge start-up so as to assure equal contents of deuterium and tritium along the current flattop, as shown in Fig. 2, left panel. The electron density during the flattop time is $\sim 5.2 \times 10^{20}$ m^{-3} and the impurity content produces an effective charge $\langle Z_{eff}\rangle \sim 1.3$. The pressure peaking factor for the onset of a sawtooth is taken to be $p_{kf} = p(0)/\langle p\rangle) > 3.0$. The first crash is considered to occur when p_{kf} is quite above 3.0, since the $q = 1$ surface enters the plasma column only at 5.3 s (See Fig. 3, left panel). The fusion gain $Q = P_{fus}/P_{input}$ and the ignition factor $f_{ign} = P_\alpha/P_{input}$, are represented in Fig. 3 (right panel). The second case (Pulse #040706d) refers to a lower tritium content, while maintaining the same total plasma density. A properly chosen RF pulse compensates for the fuel reduction (See Fig. 4, left panel) even if a delay in the alpha power production results (Fig. 4, right panel). The considered simulations point out that the ignition factor corresponds to $Q > 10$ along the current flattop. Clearly,

when ignition is attained, the thermonuclear instability is triggered and more drastic methods are needed to control it.
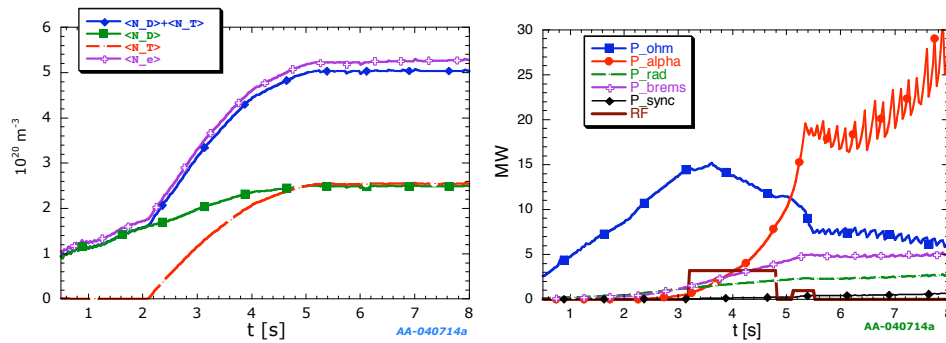

Fig. 2 - Left panel: electron and ion densities; right panel: input powers (ohmic, alpha and RF) and radiation losses.
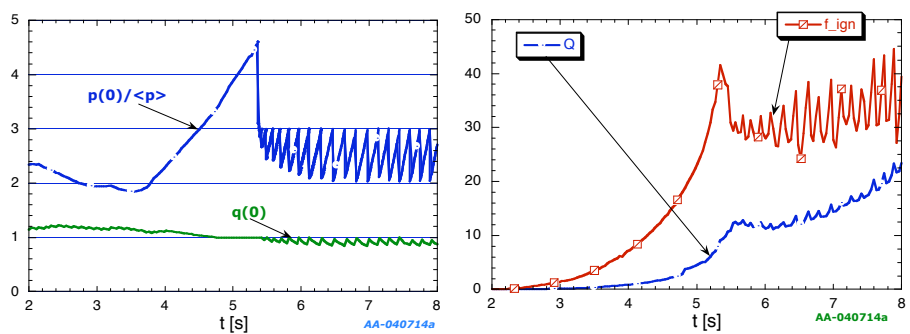

Fig. 3 - Evolution of pressure peaking factor and central safety factor (left panel). Fusion gain Q and ignition factor on the right panel.
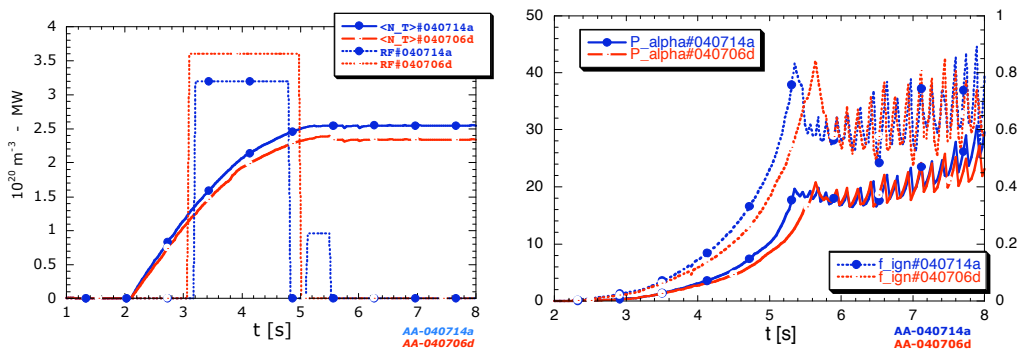

Fig. 4 - Evolution of RF power pulse and volume averaged tritium density (left panel). Alpha power and ignition factor on the right panel. Full dots mark Pulse #040714a, open dots refer to Pulse #040706d.

4. Disruption Studies

A 2D simulation of a reference disruption has been carried out using the MAXFEA code. Elongated plasmas are intrinsically subject to vertical instabilities, and because of their fast time scales, they represent a concern for the machine. It should be noted, however, that the adopted up-down symmetrical plasma confinement configuration involves operation at the so-called "neutral point", which has been shown to cause a beneficial, slower evolution of the plasma displacement [12]. This favorable circumstance has not been included in our analysis

and is considered a safety factor for the plasma chamber design. The reference plasma disruption, considered to be the worse case for the plasma chamber, is a fast downward Vertical Displacement Event (VDE): during an initial displacement the plasma current slowly decreases due to flux conservation, until the low safety factor at the edge ($q_a < 2$) triggers a rapid loss of thermal energy, followed by a fast plasma current quench (at a linear current decay rate of 2 MA/ms), with the appearance of halo currents.

The disruption produces a significant increase of electromagnetic (EM) loads requiring a non-linear transient structural analysis of the plasma chamber (PC) (Fig. 5). Static and dynamic analyses, under the EM loads produced by eddy and halo currents during a reference disruption, have been performed for a 30° sector of the PC. In order to reduce both the electromagnetic loads on the plasma chamber and the related stress during VDE's, and to increase the mechanical stiffness, a variable thickness of the plasma chamber has been adopted, ranging from 26 mm on the high field equatorial side to 52 mm on the outboard side (Fig. 6). As a result, the time constant of the plasma displacement increases up to 14 ms. Each sector of the PC joint has tapered toroidal regions in order to maintain a 26 mm welding thickness
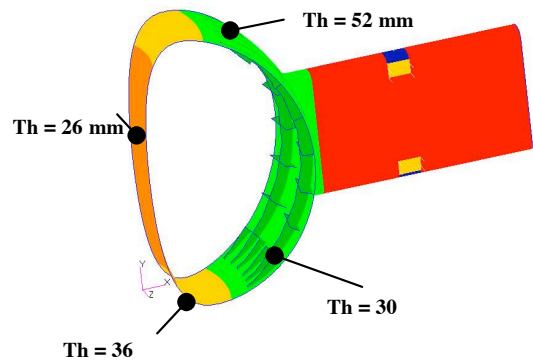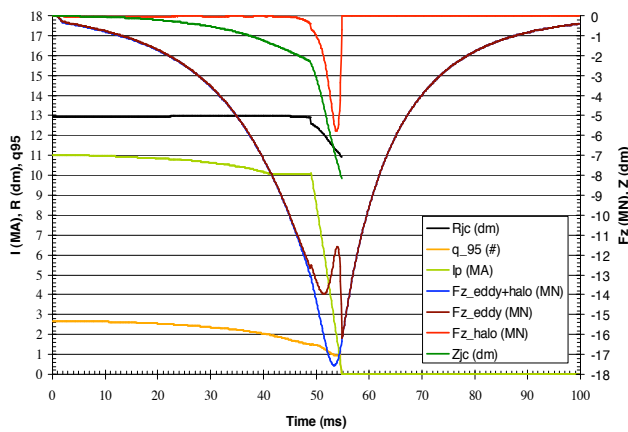

Fig. 5 - Main VDE parameters and Vertical (Fz) force due   to eddy and halo currents on plasma chamber

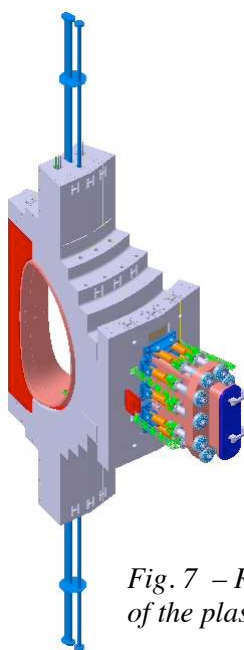Fig. 6 - Reference plasma chamber thicknesses distribution.

between adjacent sectors. The present design does not reduce the available plasma volume and maintains the original restraining system. The feasibility of one of the horizontal restraining elements of the plasma chamber has been demonstrated by the construction and test of one full size clamping sleeve (Figs. 7, 8).
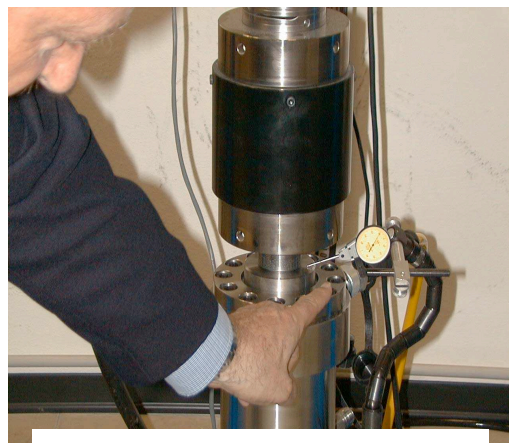

Fig. 7 – Radial support of the plasma chamber

Fig. 8 – Clamping sleeves tests

5

5. First Wall System

The design of the first wall has incorporated a new solution for the attachment of the tile carriers to the vessel that is compatible with the design of the remote handling system. The first wall is made of TZM (Molybdenum) tiles mounted on Inconel tile carrier (Fig. 9). These are attached to the plasma chamber (PC) by studs directly welded to the PC wall on the inboard side, and on plates bolted to ribs on the outboard side. Each carrier holds 8 tiles (Fig. 10) and is designed to be easily mounted and removed by the remote handling system.

In order to minimize thermal load concentrations, the tiles on each carrier are aligned with high accuracy (<0.1 mm). About 90 tile carriers cover one sector ($1/12^{th}$) of the plasma chamber, distributed over three vertical rows on the inboard side; two of them are placed symmetrically to the vertical middle plane, the other row bridges the welding joint of the two adjacent PC sectors. This arrangement prevents steps between neighbouring carriers. The studs are placed far enough from the welding and can be used to hold the welding fixtures during the assembly phase. The tile carrier assemblies can be removed also in case of seizing of the studs by shearing the notched nut heads.
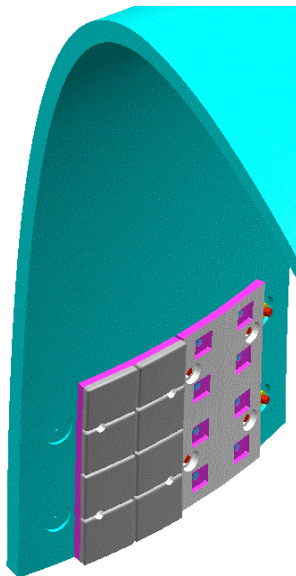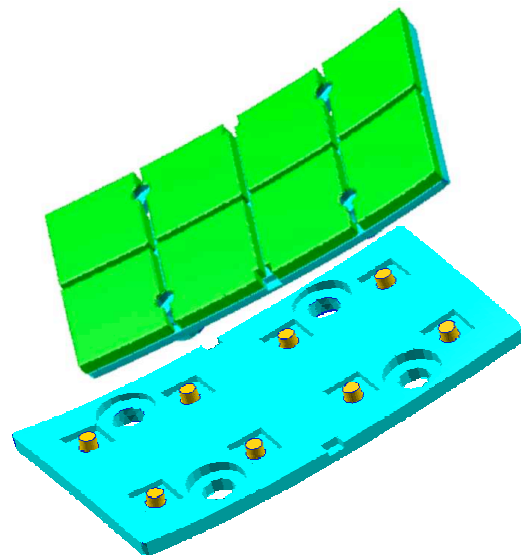

Fig. 9 - First Wall arrangement.

Fig. 10 - Typical tile carrier

The 2D analysis of the electromagnetic loads during a downward Vertical Displacement Event showed that the most loaded region is the inboard lower quarter of the poloidal cross section. A detailed 3D finite elements model of this region has been developed to deal with this problem.

6. Edge Modelling and Thermal Wall Loading

In the reference plasma configuration, the first wall acts as an extended limiter. The last closed flux surface (LCFS) matches very closely the surface of the limiter-first wall, and the resulting angle of incidence of the magnetic field lines on the material surfaces is very shallow. The presence of a tangency point between the LCFS and the solid wall means that existing codes (e.g. B2) are not suited to model the Ignitor edge [13]. In order to overcome this drawback, a finite element/finite volume approach is presently being investigated. Previous estimates of the thermal load on the first wall [14], which used some simple geometrical

approximations, have been improved by taking into account the full equilibrium for a range of energy e-folding lengths λ_E. The analysis is also being extended to some toroidally asymmetric cases: non-coincidence of the vacuum vessel and plasma main axes, misalignment of one out of the 12 first wall sectors, and vertical plasma displacements. The poloidal profile of the thermal load on first wall, including the almost isotropic contribution from the radiated fraction of input power, is reported in Fig. 11 for the toroidally and up-down symmetric limiter configuration, and for three values of λ_E (0.8 mm being the reference one). The total input power and radiated fraction are assumed to be 20 MW and 70%, respectively. In the reference high density regime of Ignitor, over 20% of the heating power is radiated, mostly by bremsstrahlung emission, from the core plasma, while a much larger fraction is effectively radiated from the outer part of the core plasma and from the scrape off layer by small amounts of intrinsic impurities (O and Mo) [14]. The resulting peak load for the reference value of λ_E is about 1 MW/m^2. This value increases by a factor of about 2 for a horizontal displacement of a single FW sector by 1 mm.
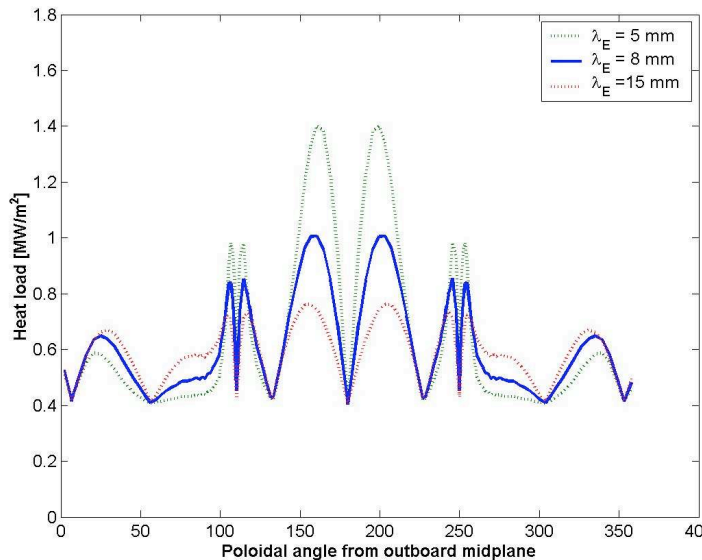

Fig. 11 - Poloidal distribution of heat loads on the first wall for the reference case of inner-wall limited plasmas with 20 MW of total heating power and 70% of radiated power, for different energy e-folding lengths (λ_E = 8 mm is the reference value).

7. Remote Handling Systems

The activation analysis for the Ignitor device indicate that the modest neutron fluence is not expected to cause serious radiation damage to most of the device components; but remote handling techniques to maintain the in-vessel components are needed. Our analyses show that a radiological lead shield located inside the cryostat and polyethylene + 5% boron collars around the horizontal ports would reduce the cooling time and allow hands-on interventions all around the machine, except for the areas facing the horizontal ports.

The remote handling (RHS) system is being designed along the lines of the one built and used in the FTU machine to install and maintain the Mo toroidal limiter. A repository file data structure integrated with the CATIA drawings from the designers of Ignitor has been developed. The relevant 3D virtual mockup software is used to see, plan and test the machine assembly sequence, the complete layout, and to simulate the operation of the remote handling system. The in-vessel RHS is based on two transporters made up of an articulated boom (Fig. 12) with end-effectors, a support structure, and a transport system. The transporters are supported by a movable structure, which can be lifted and set in position adjacent to the working horizontal ports. The structure is set level and rigidly docked to the machine. Two opposite ports will be made available for RH interventions.
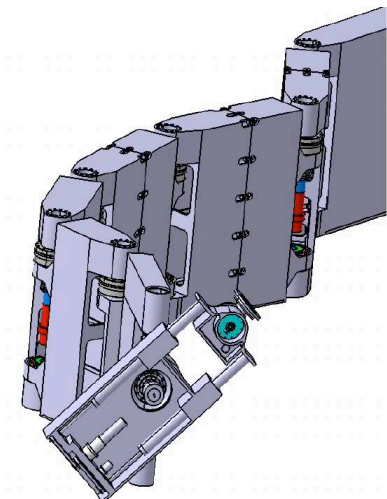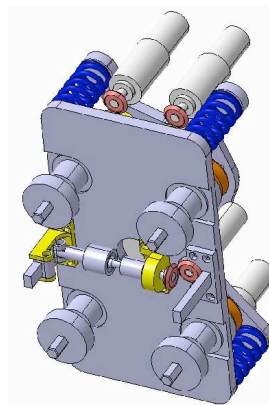
Fig.13 - End-effector for handling tile carrier.

The support structure has two different platforms; one is used to receive the sealed and shielded casks of the components removed from the vessel and the other for trays carrying the new items to be introduced. The casks are enclosed in a container in order to allow, if necessary, uncontaminated transport inside the hot cell. The transporter is provided with two TV cameras plus one optical fiber in order to inspect the wall details. Lighting will be provided through the vertical ports. The most significant end-effectors are welding and cutting tools, removal and handling tile carrier tools (Fig. 13), series of dedicated tools for diagnostics and RF antennae, vacuum cleaner, general inspection and metrology tools.

Fig. 12 - View of the articulated boom.

8. Structural Analysis of the Load Assembly

The complexity of the Ignitor machine (Core) Load Assembly and of the mechanical interactions among all its components, has led to employ a Finite Element Method ANSYS program to analyze the mechanical behavior of the structure for the most advanced operating scenarios. The Toroidal Field Coils (TFC), the Central Solenoid coils (CS), the magnetic press coils and the bracing rings materials have been all modelled by smeared mechanical and thermal properties. The in-plane and the out-of-plane load analyses have been carried out separately. Friction coefficients have been taken into account at the interfaces between the CS coils and the TFC, and between the TFC and the 316LN SS material of the C-clamps. The structural analysis is performed at the most significant times of the reference operating scenario, and include the preload at room temperature and at 30 K.

The highest stress values in the TFC are found at the end of the plasma current flat-top (t = 7.65 s, maximum electromagnetic loads), and at the end of the pulse (t = 10.35 s, no electromagnetic loads but maximum temperature). These stresses are below the yield stress of the copper material at the relevant temperature.

Since the entire machine is cooled down at 30 K, the TFC coils wedging performances are improved; this is important mainly at start-up (t = 0 sec) because the imbalance between the CS centrifugal forces and TFC centripetal ones could cause some de-wedging. The stresses in the structural components (i.e. C-clamps, Central Post) are within the ASME allowable limits at the operating temperature.

To complete the mechanical verifications, the analysis of the stresses produced by the out-of-plane loads has been performed during the toroidal field flat-top, at t = 5 s and t = 8 s. Two opposite boundary conditions were applied to the interfaces between the TFC and the surrounding structures: perfect bonding surface and perfect sliding surface. The results show

that in both cases the average shear stress acting on the TFC coil interfaces is lower than the friction reaction due to a real friction coefficient. Therefore, it is correct to model the interfaces of the TFC as perfect bonding surfaces. It is worth to note that the out-of-plane loads do not increase appreciably the values of the maximum equivalent stresses found in the in-plane load analysis except for the interlaminar shear stresses on toroidal field coils; this is the reason that justifies the decoupling of the in-plane and out-of plane load calculations. Interlaminar shear stresses values on TFC insulation are within the results of test performed at ANSALDO on small, stratified copper insulation samples.

9. Toroidal Magnet System and Cryogenic Plant

Within the Ignitor magnet system each of the 24 toroidal field coils contains 10 plates carrying up to 357.5 kA, cooled down to 30 K. The manufacturing of a first full size prototype of toroidal field coils, in spite of complying with the design requirements, brought to light some technological issues, in particular the mechanical strength of the cooling boxes of the TFC under the additional loads introduced by the adoption of a vacuum cryostat. Thus, the plate material was changed from ETP to OFHC copper, keeping the same mechanical properties but allowing for a new solution of the cooling channels. Two prototypical full size plates have been constructed, taking into account the experience gained previously. The new method of production, aimed at improving the metallurgical structure of the plates, achieves the stringent flatness requirements of the plates by a straightening operation after cold rolling and before machining. A pressure of 2 bar is applied on the turn surface to simulate the impregnation condition. Given the weldability of the material, machined welded cooling channel can be incorporated on each individual turn.

A detailed study for the cryogenic cooling system of the entire machine has been carried out by Linde Kryotechnik AG and its feasibility, using commercially available and tested components, has been confirmed. Helium gas is used for cooling the poloidal field coils and the toroidal field magnet to 30 K. The inter-pulse cooling time is about 5 hours for the highest plasma current pulse (11 MA).

The cooling of the rest of the machine is assured by the good thermal contacts between the major components.
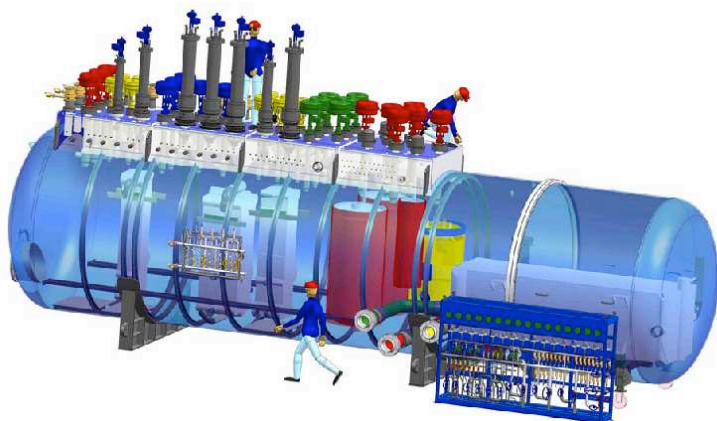
The plasma chamber requires a dedicated cooling system. The cryogenic plant design has been developed to perform the first cool-down of the entire machine from ambient temperature, to re-cool the magnets to the initial temperatures after a current pulse, and to warm-up the machine to ambient temperature.

The layout of the equipments included in the cold-box (length: 12 m; diameter: 3.5 m; total height: 6 m; weight: 60 t) has been specified as exemplified in Fig.14.

Fig. 14 – Cold-box layout.

10. ICRH and Electrical Diagnostic Systems

The previous transport simulations of burning plasma scenarios show that modest amounts of ICRH heating are required to achieve the desired performances. For this reason, only four antennas (the basic module being two antennas) will be installed at the beginning, aiming at delivering 7 to 10 MW to the plasma at frequencies at 120 and 70 MHz, respectively, occupying four horizontal ports. The other two ports originally devoted to the ICRH systems will remain available for future use. A major improvement in the ICRH antenna design is represented by the compatibility of all in-vessel components with the remote handling system, thus allowing for installation, maintenance, and upgrading during the active life of the experiment. In particular, the Faraday shield design has been completed and fully integrated with the "new" plasma chamber and first wall system. The conceptual design of the ICRH generation and distribution system (including the high vacuum transmission line, HVTL, inside the ports of the machine) has been also defined. In order to perform full-phasing - in both poloidal and toroidal directions – between the RF waves launched by the antenna's straps, the power generated by a RF source is divided between two antenna's straps located in two different ports. RF wave phasing is controlled by regulating the generator phase and by means of dedicated components included in the RF transmission system.

A significant R&D effort has been undertaken to test the materials and manufacturing processes of the electrical diagnostics system, which has been designed as a system fully integrated with the plasma chamber and the first wall.

11. Poloidal Field System and Electrical Power Supply Optimization

The most appropriate current distribution within the Poloidal Field (PF) coils has been identified and the coil geometry modified, easing the requirements on the power supplies and on the adopted materials. In particular, the use of Dispersion Strengthen Copper has been shown to be avoidable because more uniform temperature and stress distributions were obtained, mainly by increasing the conductor cross sections and reducing the diameters of the cooling channels in the coils forming the central solenoid, and thus decreasing the current density where the field is highest. An iterative optimization process of the complete power supply system has been carried out, leading to the identification of a new reference plasma current pulse at 11 MA over a 4 s flat top.

The total installed power (defined as $V_{max} \times I_{max}$) is now about 2400 MVA instead of about 3300 MVA estimated before the optimization process. The peak power supplied by the 400 kV Grid is about 1000 MVA including 480 MVAr of reactive power locally generated by thyristor static VAR compensators (SVC). The appropriate government authority (GRTN) has carried out an in-depth analysis of the connection of the Ignitor power supply to the Rondissone node (near Turin). The power requirements (max active power, max reactive power, max active power negative/positive steps) were found to be consistent with the European 400 kV grid operational requirements [15] and the connection has been authorized. The detailed designs of the SVC, of the current harmonics filtering units and of the thyristor power amplifiers of the IGNITOR coils have been completed. In the context pf the overall plant layout, all the power supply components are designed as of the outdoor kind. In particular, the power amplifiers, together with all power control and conditioning systems, are located inside standard containers that are electrically connected with the loads by means of outdoor, segregated bus-bars.

[1]   B. Coppi, A. Airoldi, F. Bombarda et al, *Nucl. Fusion* **41**, 1253 (2001).

[2]   A.Airoldi and G.Cenacchi, *Nucl. Fusion* **37**, 1117 (1997).

[3]   A.Airoldi and G.Cenacchi, *Nucl. Fusion* **41**, 687 (2001).

[4]   D. Frigione, E. Giovannozzi, C. Gormezano, et al., *Nucl. Fusion* **41**, 1613 (2001).

[5]   F. Bombarda, et al., 31st EPS Conf. on Plasma Phys. London, ECA Vol.28G, P-2.119 (2004).

[6]   B. Esposito, M. Marinucci, M. Romanelli et al, submitted to *Plasma Phys. Control. Fusion* (2004).

[7]   A. Frattolillo, S. Migliori, et al., http://www.aps.org/meet/DPP03/baps/abs/S2080045.html .

[8]   Y. Shimomura et al., *Plasma Phys. Control. Fusion* **43**, A385 (2001).

[9]   G. Vlad, et al., *Nucl. Fusion* **41**, 687 (2001).

[10] G. Bracco, et al., 17th IAEA Fusion Energy Conf., Yokohama,1998, (Vienna: IAEA), Paper XP2/01, http://www.iaea.org/programmes/ripc/physics/html/node128.htm.

[11] A.Airoldi and G. Cenacchi, IFP Report FP 03/8 (2003).

[12] Y. Nakamura et al., 19th IAEA Fusion Energy Conf. , Lyon, 2002, (Vienna: IAEA), Paper EX/P4-13, http://www.iaea.org/programmes/ripc/physics/fec2002/pdf/exp4_13.pdf.

[13] F. Subba, and R. Zanino, "Modeling plasma-wall interactions in First-Wall Limiter geometry", to be published in *Comp. Phys. Comm.* (2004).

[14] R. Zanino and C. Ferro, *Contrib. Plasma Phys.* **36**, 260 (1996).

[15] D. Baraldi, B. Coppi, M. Salvetti et al., *AEI* **90** (12), 2003.